Targeting Fibroblast Activation Protein for Molecular Imaging of Fibrotic Remodeling in Pulmonary Arterial Hypertension

Peng Hou*[1], Haiming Chen*[2], Sihao Liang*[1], Wenliang Guo*[2], Ruiyue Zhao*[1], Huailu Pan*[2], Haimin Liu[2,3], Youcai Li[1], Jie Lv[1], Kaixiang Zhong[1], Miao Ke[1], Yimin Fu[1], Huizhen Zhong[1], Xinlu Wang[1], and Cheng Hong[2]

[1]Department of Nuclear Medicine, First Affiliated Hospital of Guangzhou Medical University, Guangzhou, China; [2]Department of Pulmonary and Critical Care Medicine, First Affiliated Hospital of Guangzhou Medical University, Guangzhou Institute of Respiratory Health, State Key Laboratory of Respiratory Disease, National Clinical Research Center for Respiratory Disease, Guangzhou, China; and [3]Department of Critical Care Medicine, Heyuan People's Hospital, Heyuan, China

The purpose of this study was to investigate the feasibility of using ^{18}F-labeled fibroblast activation protein inhibitor (FAPI) PET/CT in assessing the fibrotic remodeling of the pulmonary artery (PA) and the right ventricle (RV) in pulmonary arterial hypertension (PAH). **Methods:** In a rat model of monocrotaline-induced PAH, rats were euthanized at different time points for tissue analysis (fibroblast activation protein immunofluorescence and Masson's trichrome staining) after completing ^{18}F-FAPI PET/CT and hemodynamic measurements. Thirty-eight PAH patients were enrolled to participate in ^{18}F-FAPI PET/CT imaging, with right heart catheterization and echocardiography performed within 1 wk to assess pulmonary hemodynamics and cardiac function. **Results:** In the animal experiments, RV systolic pressure in monocrotaline rats increased from day 14 to day 21 after injection. ^{18}F-FAPI uptake and fibroblast activation protein expression in the myocardium and lungs peaked on day 14 after injection. Collagen deposition in the RVs and peripheral PAs of monocrotaline rats progressively deteriorated from day 14 to day 21. In the human PAH study, ^{18}F-FAPI PET/CT imaging identified varying degrees of ^{18}F-FAPI uptake in the myocardium and proximal and distal PAs, correlating with clinical, RV function, and pulmonary hemodynamic parameters. Among the 5 follow-up patients who underwent a second ^{18}F-FAPI PET/CT scan after 6 mo (range, 4–9 mo) of PAH-targeted therapy, 3 demonstrated reduced ^{18}F-FAPI uptake, corresponding with clinical improvement. **Conclusion:** ^{18}F-FAPI PET/CT imaging is feasible for visualizing the remodeling of the PA and the RV in PAH. Although it offers promise for assessing disease-related changes, its role in evaluating disease severity and monitoring therapeutic efficacy requires further investigation.

Key Words: ^{18}F-FAPI; PET/CT; pulmonary arterial hypertension; right ventricle; pulmonary artery

J Nucl Med 2025; 66:98–103
DOI: 10.2967/jnumed.124.268376

Pulmonary arterial hypertension (PAH) is a progressive and life-threatening disease characterized by progressive pulmonary arterial remodeling (*1*). Heightened activation of adventitial fibroblasts of the pulmonary artery (PA) drives vascular remodeling, leading to disease progression and contributing to right ventricle (RV) afterload and cardiac dysfunction (*2*). Activation of cardiac fibroblasts is similarly intensified during this process (*3*,*4*). In this context, fibroblast activation is a common pathophysiologic trait in both PAs and right heart remodeling in PAH (*5*). Consequently, early detection and assessment of fibroblast activation in PAH may allow timely intervention and may help prevent irreversible remodeling, thus improving patients' prognosis. Histopathologic examination is the gold standard for assessing fibrotic remodeling in PAH, but tissue acquisition is an invasive procedure, and it is usually difficult to obtain relevant tissue samples before the end stage of PAH.

Activated fibroblasts are key mediators of tissue remodeling, with a distinctive feature being the expression of fibroblast activation protein (FAP). FAP is a type II integral membrane glycoprotein, expressed in activated fibroblasts but not in their quiescent counterparts (*6*). Therefore, its specific quantitative evaluation can help detect fibroblast activation at an early stage. Recent studies have used radionuclide-labeled FAP inhibitors (FAPIs) to image the RV and PA in chronic thromboembolic pulmonary hypertension and the RV in PAH (*7*–*9*), demonstrating the potential of FAPI PET imaging for assessing fibroblast activation in the RV and PA. Although PA remodeling is a hallmark of PAH, the use of FAPI PET imaging to evaluate PA remodeling in PAH patients has not been previously explored, to our best knowledge. Additionally, the correlation between FAPI uptake in the right side of the heart, PA, and histopathologic findings in PAH remains unclear.

In this study, we investigated the potential utility of FAPI PET/CT in PAH. Given that monocrotaline (hereinafter referred to as MCT) causes direct endothelial damage and vascular remodeling and can induce the occurrence of severe and lethal PAH, which ultimately leads to RV hypertrophy (*10*), an MCT-induced rodent model was used in the study. First, serial ^{18}F-FAPI-42 (hereinafter referred to as ^{18}F-FAPI) PET/CT imaging was performed on an MCT-induced PAH rat model, and the imaging findings were correlated with histopathologic changes at different time points. Second, ^{18}F-FAPI PET/CT imaging of PAH patients was prospectively analyzed in correlation with pulmonary hemodynamic, echocardiographic, and clinical parameters.

MATERIALS AND METHODS

Overall Study Design of Animal Experiment

All experimental protocols were approved by the Animal Care and Use Committee of Affiliated First Hospital of Guangzhou Medical

Received Jul. 8, 2024; revision accepted Dec. 2, 2024.
For correspondence or reprints, contact Cheng Hong (gyfyyhc@126.com) or Xinlu Wang (71lu@163.com).
*Contributed equally to this work.

University (ID 2022481). Twenty male Sprague–Dawley rats (200 ± 20 g) were obtained from Guangdong Medical Laboratory Animal Center (Guangzhou, China) and randomly divided into 2 groups: the MCT group (n = 15) and the control group (n = 5). PAH was induced on day 0 by a single subcutaneous injection of MCT (50 mg/kg; MedChemExpress; HY-N0750). After the injection, the MCT group underwent ^{18}F-FAPI PET/CT scans and hemodynamic measurement and were euthanized at 3 time points: day 7, 14, or 21 (n = 5 for each subgroup; Fig. 1A). Additionally, the control group underwent FAPI PET/CT scans on days 0, 7, 14, and 21 and were euthanized after hemodynamic measurement on day 21.

Small-Animal PET/CT Imaging

All rats were scanned with ^{18}F-FAPI PET/CT on a MadicLab PSA071 PET/CT scanner (Shandong Madic Technology Co., Ltd.), with an acquisition time of 10 min. The entire procedure was performed with the rat sustained with 1.5% isoflurane in oxygen anesthesia. PET/CT scans were performed for all rats 40–50 min after the tail vein injection of ^{18}F-FAPI at a dosage of 7.4 ± 1.8 MBq/0.2 mL. PET image reconstruction was performed as described previously (*11*). PET/CT images were reconstructed with a 3-dimensional row action maximum likelihood algorithm with a CT scan (80 kV, 70 mAs) for attenuation correction and fusion localization, with 0.8 mm × 0.8 mm × 0.8 mm as the final resolution. The degree of ^{18}F-FAPI uptake was quantified by delineating the region of interest in the heart, lungs, and reference tissue (muscle in the left foreleg) on the coregistered transaxial PET/CT images, and SUV ratios were calculated by target uptake and reference uptake (muscle).

Details of the hemodynamic measurement, tissue harvesting, Masson's trichrome staining, and immunofluorescence staining are described in the supplemental materials (available at http://jnm.snmjournals.org) (*12*,*13*).

Study Population

The study was performed in line with the principles of the Declaration of Helsinki and was approved by the Ethics Committee of the First Affiliated Hospital of Guangzhou Medical University (ID 2021-23), and all patients provided written informed consent. From August 2022 to November 2023, patients were prospectively and consecutively recruited. Inclusion criteria included patients who were aged 18–80 y, patients who were diagnosed with PAH by right heart catheterization (RHC) to have a mean PA pressure greater than 20 mm Hg according to the guidelines (*1*), patients who underwent RHC and echocardiography within 1 wk of the ^{18}F-FAPI PET/CT scan, and patients for whom there was no significant change in condition and clinical treatment during this interval. Exclusion criteria included patients having interstitial lung disease, having a tumor, being pregnant and breastfeeding, having an unwillingness to participate, and experiencing technical failures or incomplete imaging. All patients were subjected to complete history tacking, clinical evaluation, imaging and laboratory tests, and RHC.

Furthermore, a group of control subjects (n = 17) was selected from our patient database to establish the reference range of ^{18}F-FAPI uptake in the RVs and PAs. The inclusion criteria of controls are shown in Supplemental Data 2.

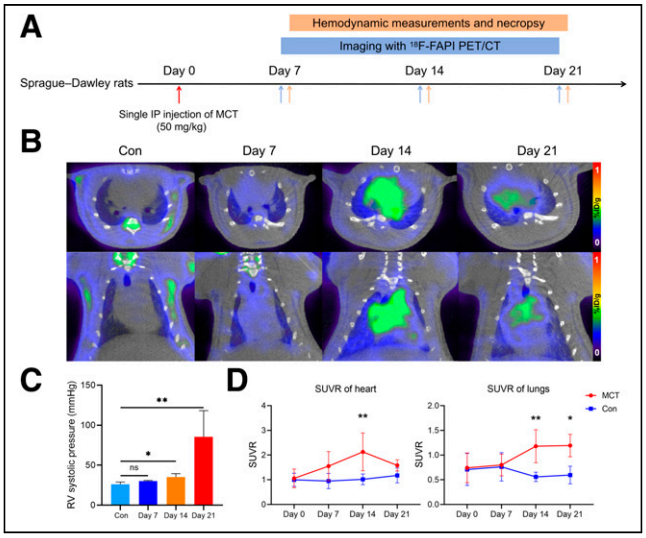

FIGURE 1. Time course of PAH progression and ^{18}F-FAPI uptake of myocardium and lung in MCT rats. (A) Schematic diagram of animal experiment. (B) Series of sequential ^{18}F-FAPI PET/CT images (transverse plane and coronal plane) of MCT-induced PAH model. (C) RV systolic pressure progressively increased with progression of PAH, showing significant difference starting from day 14. Kruskal–Wallis test was performed. (D) Changes of ^{18}F-FAPI uptake in MCT rats at different time points. Two-way ANOVA was used between MCT and control groups. Control group (Con) day 7 and day 14: n = 5; day 21: n = 3 (A–D). *P < 0.05, **P < 0.01, ns = no significance. IP = intraperitoneal; SUVR = SUV ratio.

PET/CT Image Analysis

All PET/CT images were independently interpreted by 2 experienced nuclear medicine physicians (with 30 and 10 y of experience in PET reading) who were masked to the clinical and other imaging results. In the event of a disagreement, scans were jointly reviewed to reach a consensus. PET images were analyzed on a nuclear medicine information system (Beijing Mozi Healthcare Ltd.). ^{18}F-FAPI uptake in the myocardium, PA, and liver was separately evaluated using qualitative (visual) and semiquantitative analyses. The PAs were anatomically divided into 1 main PA (main PA trunk, left PA, and right PA), 5 lobar PAs, and 18 segmental PAs. Lesions involving main or lobar PAs were considered to be proximal, and those involving segmental and subsegmental PAs were considered to be distal (*14*). For visual analysis, ^{18}F-FAPI uptake in the myocardium, PA wall, or liver higher than in the blood pool (superior vena cava) was defined as abnormal. For semiquantitative analysis, using PET- and CT-fused images, the lesions were automatically segmented and outlined using a 3-dimensional regional growth algorithm, and the SUV_{max} was recorded. Additionally, a circular region of interest (5 mm in diameter) was placed in the cavity of the superior vena cava, and the SUV_{mean} was recorded as the background activity before the target-to-background ratio was calculated.

Comprehensive details on ^{18}F-FAPI PET/CT imaging, semiquantitative analysis of ^{18}F-FAPI uptake in the myocardium, PAs, and liver, along with information on RHC and echocardiography are provided in Supplemental Data 2.

Statistical Analysis

Data were analyzed using SPSS 26.0 (SPSS Inc.). The Mann–Whitney U test and χ^2 test were used to compare the differences between groups. Statistical comparison of ^{18}F-FAPI uptake changes was determined between the MCT group and the control group using 2-way ANOVA and a Bonferroni posthoc test. Comparisons over time within the MCT rat group were tested with 1-way ANOVA followed by a Bonferroni posthoc test or Kruskal–Wallis test as appropriate. Spearman correlation analysis was conducted to explore the correlation of ^{18}F-FAPI uptake with clinical, RV functional parameters, and hemodynamic parameters. A P value of less than 0.05 was considered statistically significant.

RESULTS

Changes of ^{18}F-FAPI Uptake and Hemodynamics in MCT Rats

In this study, 2 MCT rats died during hemodynamic measurement on day 21, and their data were excluded. Figures 1B–1D

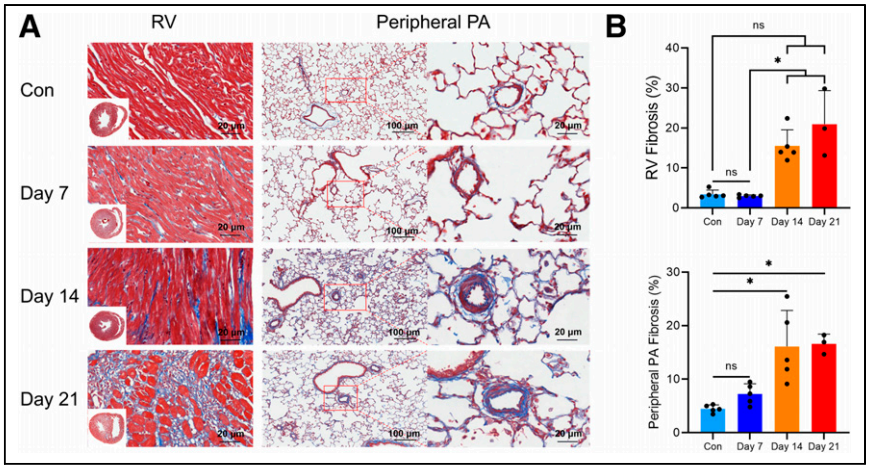

FIGURE 2. Fibrosis pattern of RV and peripheral PA in MCT rats. (A) Representative images of Masson's trichrome–stained RV and lung sections during corresponding intervals (collagen in blue). Scale bar represents 20 and 100 μm, respectively. (B) Planimetric quantifications of fibrosis (blue areas stained by Masson's trichrome over total tissue surface in percentage) showed gradual increase in fibrosis of RV and peripheral PA in MCT rats. Kruskal–Wallis test was performed. Control group (Con) day 7 and day 14: $n = 5$; day 21: $n = 3$ (A and B). *$P < 0.05$, ns = no significance.

illustrate the changes of ^{18}F-FAPI uptake and hemodynamics. On day 7 after injection, ^{18}F-FAPI uptake slightly increased in the myocardium (SUV ratio, 1.55 ± 0.59 vs. 0.95 ± 0.31, $P = 0.1346$) and lung (SUV ratio, 0.80 ± 0.22 vs. 0.76 ± 0.29, $P = 0.9989$) in the MCT group compared with controls. A significant increase was observed on day 14 (myocardium: 2.13 ± 0.76 vs. 1.02 ± 0.22, $P = 0.0013$; lung: 1.18 ± 0.33 vs. 0.56 ± 0.09, $P = 0.0028$), peaking before a decrease by day 21, but values remained higher than in the controls (myocardium: 1.58 ± 0.23 vs. 1.17 ± 0.30, $P = 0.5998$; lung: 1.18 ± 0.33 vs. 0.60 ± 0.18, $P = 0.0144$). Compared with those of the controls, hemodynamic measurements revealed no significant change in RV systolic pressure in the MCT group on day 7, but it was elevated by day 14 and increased more rapidly between days 14 and 21, diverging from the ^{18}F-FAPI uptake trends in the myocardium and lungs.

Histology and Immunofluorescence Assay

Masson's trichrome staining (Fig. 2) revealed significant collagen deposition in the RV and peripheral PA of MCT rats, progressively increasing from day 7 to day 21 after injection. Although no significant difference in cardiac fibrosis was observed between MCT rats and controls, an increase in cardiac fibrosis was noted in MCT rats from day 14 to day 21, indicating heightened fibrotic activity.

Immunofluorescence analysis (Fig. 3) also revealed pronounced FAP expression in the RV and peripheral PA of MCT rats. By day 14, FAP fluorescence intensity in the MCT group was significantly higher than on day 7 and higher than in the control group, consistent with FAPI uptake changes in PET/CT. The majority of FAP-positive cells in the RV and peripheral PA expressed vimentin (Supplemental Fig. S1). The colocalization of vimentin with FAP suggests the accumulation of activated fibroblasts in fibrotic tissues after MCT injection.

Patient Characteristics

The clinical characteristics of 38 PAH patients are presented in Supplemental Table 1. The patients were relatively young (mean age, 34 ± 11 y) and predominantly female (25/38, 65.8%). The median duration of symptoms preceding diagnosis was 24 mo (range, 12–51 mo). Patients' RV systolic functional parameters were close to the lower limits of normal. They had increased mean PA pressure (57.2 ± 16.9 mm Hg) and pulmonary vascular resistance (10.6 ± 5.7 Wood units). The common types of PAH in this cohort were idiopathic PAH (23/38, 60.5%) and PAH associated with congenital heart disease (10/38, 26.3%). Most patients received dual (14/38, 36.8%) or triple (18/38, 47.4%) PAH-targeted therapy.

^{18}F-FAPI PET/CT Uptake in PAH Patients

In the control group, none of the subjects showed increased ^{18}F-FAPI uptake in the RVs or PAs (Supplemental Fig. S2). In contrast, 97.4% (37/38) of PAH patients showed visually increased ^{18}F-FAPI in both RV and PAs (Fig. 4A). Abnormal ^{18}F-FAPI uptake was also observed in the right atrium (25/38, 65.8%), left ventricle (15/38, 39.5%), left atrium (4/38, 10.5%), and liver (3/38, 7.9%). At the vascular level, the prevalence of increased ^{18}F-FAPI uptake in the main, lobar, and segmental PAs was 97.4% (37/38), 86.8% (165/190), and 59.2% (405/684), respectively. Figure 4D and Supplemental Figure S3 show the ^{18}F-FAPI uptake in the corresponding region.

Semiquantitative analysis revealed significantly higher ^{18}F-FAPI uptake in the RV and PAs of PAH patients compared with controls (Figs. 4B and 4C). Among PAH patients, ^{18}F-FAPI

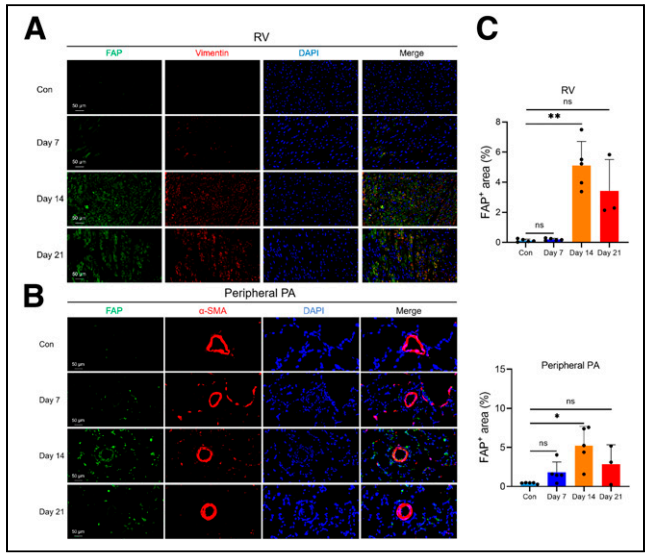

FIGURE 3. FAP immunofluorescence staining of RV and peripheral PA in MCT rats. (A) Representative images of FAP immunofluorescence staining of RV sections during corresponding intervals (FAP, green; vimentin, red; 4′,6-diamidino-2-phenylindole [DAPI], blue). Scale bar represents 50 μm. (B) Representative images of FAP immunofluorescence staining of lung sections during corresponding intervals (FAP, green; α-smooth muscle actin [α-SMA], red; DAPI, blue). Scale bar represents 50 μm. (C) FAP expression in RV and peripheral PA reached its peak on day 14 and began to decrease on day 21. Control group (Con) day 7 and day 14: $n = 5$; day 21: $n = 3$. *$P < 0.05$, Kruskal–Wallis test; ns = no significance.

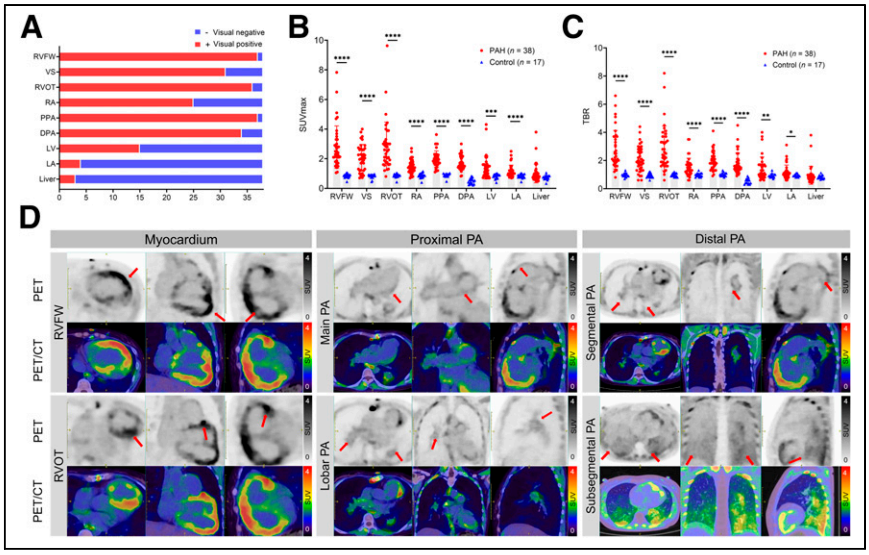

FIGURE 4. Visual qualitative assessment and semiquantitative analysis of thoracic PET/CT images. (A) Visual assessment results of PAH patients. RVFW and proximal PA (PPA) exhibit highest positivity rate for ^{18}F-FAPI uptake (37/38, 97%). In addition to right side of heart and PAs, uptake of ^{18}F-FAPI was also observed in left ventricle (LV), left atrium (LA), and liver. (B and C) SUV_{max} and target-to-background ratio (TBR) of myocardium and PAs in PAH patients was significantly higher than that in control subjects. Differences between groups was calculated with Mann–Whitney *U* test. (D) Representative ^{18}F-FAPI PET/CT images in PAH patients. 35-y-old female patient with PAH associated with congenital heart disease and impaired RV function (RV fractional area change, 14.3%; tricuspid annular plane systolic excursion, 11 mm) showed significant uptake of ^{18}F-FAPI in RVFW (SUV_{max}, 6.5, red arrows) and RVOT (SUV_{max}, 5.0, red arrows). Her enlarged proximal PAs (SUV_{max}, 5.0, red arrows) and segmental PAs (SUV_{max}, 5.0, red arrows) also exhibited increased ^{18}F-FAPI uptake. 58-y-old female patient of idiopathic PAH presenting decreased RV function (RV fractional area change, 16.7%; tricuspid annular plane systolic excursion, 16 mm) showed diffuse mild ^{18}F-FAPI uptake in subsegmental and below levels of PAs (SUV_{max}, 3.0, red arrows), with no abnormalities observed in corresponding areas on CT (Supplemental Fig. S3). $^{*}P < 0.05$, $^{**}P < 0.01$, $^{***}P < 0.001$, $^{****}P < 0.0001$. DPA = distal PA; RA = right atrium; VS = ventricular septum.

uptake (SUV_{max}/target-to-background ratio) of the RV free wall (RVFW) and RV outflow tract (RVOT) was significantly higher than that in other sites.

Correlation Between ^{18}F-FAPI and Clinical, RV Function, and Pulmonary Hemodynamic Parameters

As shown in Supplemental Figures S4 and S5, in PAH patients, the SUV_{max} of the RVFW, ventricular septum, and RVOT was positively correlated with mean right atria pressure and pulmonary vascular resistance (all $P < 0.05$) and negatively correlated with cardiac output, cardiac index, and mixed venous oxygen saturation (all $P < 0.05$). Echocardiography showed a negative correlation between RV fractional area change and SUV_{max} in the RVFW and ventricular septum (all $P < 0.05$). Clinically, the SUV_{max} of the RVFW, RVOT, right atrium, proximal PA, and distal PA was positively correlated with the World Health Organization functional class (all $P < 0.05$). Additionally, the SUV_{max} of the RVFW, ventricular septum, and RVOT was positively correlated with the N-terminal pro brain natriuretic peptide (all $P < 0.05$). Supplemental Figure S6 presents the correlation between the target-to-background ratio index and clinical, RV function, and pulmonary hemodynamic parameters.

Associations Between Baseline ^{18}F-FAPI Uptake and Changes in Clinical Parameters During Follow-up

Thirty-eight PAH patients were followed for 13 mo (range, 11–19 mo) and categorized as either stable or progressors on the basis of clinical deterioration criteria (Supplemental Fig. S7). Twenty-eight patients (73.7%) were considered stable and 10 as progressors (26.3%). Progressor patients presented significantly higher baseline ^{18}F-FAPI uptake of the main PA than did the stable patients (2.0 ± 0.4 vs. 1.6 ± 0.4, $P = 0.0217$). No significant differences in ^{18}F-FAPI uptake were observed in other parts between progressors and stable patients.

Treatment Response Assessment Using ^{18}F-FAPI PET/CT

After 6.0 mo (range, 4.0–9.0 mo) of PAH-targeted therapy, 5 follow-up PAH patients underwent a second ^{18}F-FAPI PET/CT scan. The results indicated a decrease in ^{18}F-FAPI uptake in 3 patients, an increase in 1 patient, and a wider range of uptake in 1 patient. Overall, the trend of ^{18}F-FAPI uptake is consistent with the change of the patient's condition. Two patients with no improvement in ^{18}F-FAPI uptake were in line with clinical deterioration criteria compared with baseline (Fig. 5; Supplemental Table 2).

DISCUSSION

The major findings of our study include the following: (1) Multiple time-point ^{18}F-FAPI PET/CT in MCT rats revealed early uptake of FAPI in the myocardium and PAs, consistent with the heightened FAP expression and collagen deposition, indicating its ability to detect early remodeling in experimental PAH; (2) in PAH patients, FAP activity in the right heart and PAs was elevated and correlated with multiple clinical, RV function, and pulmonary hemodynamic parameters; and (3) ^{18}F-FAPI uptake in the right heart and PAs decreased after PAH-targeted therapy, suggesting the potential reversibility of fibroblast activation in PAH. These findings indicate that ^{18}F-FAPI PET/CT can noninvasively and quantitatively visualize the fibroblast activation in PAH, offering a novel approach for disease evaluation.

Previous studies have demonstrated the feasibility of ^{68}Ga-FAPI PET for detecting early cardiac fibroblast activation in heart failure (*15*). In vitro cultivation of pulmonary vascular cells from both PAH patients and animal models revealed early and substantial proliferation of adventitial fibroblasts, along with the perpetuation of their abnormal or consistently activated cellular phenotypes (*2*,*16*). In this study, ^{18}F-FAPI uptake in the myocardium and peripheral PAs of MCT rats peaked on day 14 and then gradually decreased, a result supported by immunofluorescence staining. Immunofluorescence showed FAP colocalized with fibrosis-related marker vimentin in the myocardium and peripheral PAs, confirming the accumulation of activated fibroblasts in fibrotic tissues after MCT-induced PAH. Contrary to FAP expression changes, Masson's staining showed that fibrosis in the myocardium and peripheral PAs commenced on day 14 and progressed over time. Thus, ^{18}F-FAPI might be a useful tool to visualize early PAH progression.

PA fibroblasts represent a pivotal cell component of the adventitia. In response to vascular stimulation, PA fibroblasts are highly

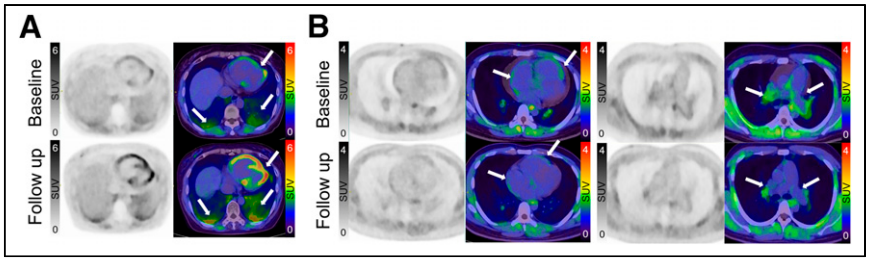

FIGURE 5. Representative images of ^{18}F-FAPI PET/CT at baseline and follow-up. 58-y-old female patient with idiopathic PAH exhibited no improvements after 7 mo of dual PAH-targeted drug therapy. Follow-up ^{18}F-FAPI PET/CT demonstrated increased uptake of ^{18}F-FAPI in the RVOT, RV, left ventricle, and subsegmental PAs compared with baseline (arrows). (B) 23-y-old male patient with idiopathic PAH exhibited significant improvements after 3 mo of triple PAH-targeted drug treatment. Follow-up ^{18}F-FAPI PET/CT results showed decreased ^{18}F-FAPI uptake in the right atrium, RV, RVOT, and proximal PAs compared with baseline (arrows).

activated and undergo phenotypic transformation characterized by hyperproliferation, migration, and inflammatory activities, promoting adventitia remodeling in PAH (*2*,*17*). Increased mechanical stress and pressure overload from PAH can lead to adaptive fibrosis of the RV (*18*). RV dysfunction leads to venous congestion and reduced perfusion, both of which can cause solid organ injury. Understanding the whole organ axis and its progression affected by PAH may provide insights into the optimal timings of intervention. In this study, we detected the FAPI signal from the PA tree, RV, and even the liver in PAH, suggesting that PAH has widespread systemic manifestations. Additionally, RV dilation adversely impacts the interaction between the left ventricles and RVs. We also observed a slight increase in ^{18}F-FAPI uptake in the left ventricle and left atrium, implying that PAH patients may experience fibrotic changes in other parts of the myocardium, potentially leading to global heart failure. However, since this study included different PAH subtypes and patients undergoing PAH-targeted therapy, how the signals in these tissues relate to each other, to the time course, and to other markers of disease severity remains unclear and warrants further investigation in a larger PAH patient cohort.

This study found correlations between FAPI uptake and multiple clinical, pulmonary hemodynamic, and echocardiographic indicators, suggesting that ^{18}F-FAPI uptake may serve as an indicator of PAH severity. RV fractional area change and tricuspid annular plane systolic excursion are classic indices of RV function in echocardiography. We observed a negative correlation between FAPI uptake in RV and RV fractional area change but no significant correlation with tricuspid annular plane systolic excursion, similar to the findings in chronic thromboembolic pulmonary hypertension (*8*). This suggests that ^{18}F-FAPI uptake in the RV may reflect overall RV systolic function. However, unlike previous studies, there was no correlation between ^{18}F-FAPI uptake and tricuspid annular plane systolic excursion, potentially due to differences in study subjects, patient numbers, and disease severity. Additionally, baseline ^{18}F-FAPI uptake trended higher in PAH patients who experienced clinical deterioration during follow-up, though the difference was not statistically significant. Given the small patient sample and short follow-up period, larger studies with more patients and longer follow-up are needed to evaluate the prognostic value of ^{18}F-FAPI uptake for PAH.

In PAH, stimuli such as shear stress, hypoxia, and inflammation promote fibroblast activation (*19*). Although fibroblast activation is typically self-limited during acute tissue repair, its persistence in progressive PAH remains unclear, especially regarding the potential effects of PAH-targeted drugs on fibroblast activation. Although these drugs primarily focus on pulmonary vasoconstriction rather than vascular remodeling, they can still influence the RV by reducing RV afterload. Preclinical studies indicate that phosphodiesterase 5 inhibition reduces interstitial fibrosis in PAH animals with established RV dysfunction (*20*). Furthermore, treatment with inhaled iloprost partially reverses established RV fibrosis by preventing collagen synthesis and decreasing cardiac fibroblast activation (*21*). These findings suggest that PAH-targeted drugs may also impact fibroblast activation. Our limited follow-up ^{18}F-FAPI PET/CT scans showed decreased ^{18}F-FAPI uptake in 3 patients who experienced clinical improvement, suggesting a certain reversibility of fibroblast activation. However, increased ^{18}F-FAPI uptake was observed in 2 patients with limited improvement. We postulate that vasodilators may be more effective in early PA remodeling, whereas advanced cases may develop resistance to treatment (*22*). Thus, although further studies are needed to verify these findings, ^{18}F-FAPI PET/CT holds potential as a noninvasive tool for monitoring treatment response.

Our study has several limitations. First, only the MCT–PAH model was used in animal experiments; other models, such as the Sugen 5416/hypoxia-induced PAH model, should be explored to determine whether early ^{18}F-FAPI uptake can be observed across different PAH models and to assess whether therapeutic intervention at the early FAP signal stage is more effective than at later stages, as well as its impact on tissue expression and FAP levels. Second, the limited data at day 21 due to animal loss may affect the accuracy of our assessment of peak FAPI uptake activity at that time point. Third, the small and heterogeneous participant group, with most patients undergoing RHC and receiving PAH-targeted therapy before PET/CT scanning, may lead to bias in baseline SUV measurements. Additionally, we did not obtain patient specimens for pathologic confirmation. Lastly, the thin PA wall made the SUV measurement susceptible to partial-volume effects. Although we used a high-resolution PET imaging protocol to minimize the influence of partial-volume effects, it remains a critical factor to consider when interpreting our results. Future research should further investigate partial-volume effects across various anatomic regions and evaluate enhancements in imaging technologies to improve the accuracy of quantitative analyses.

CONCLUSION

^{18}F-FAPI PET/CT can detect fibroblast activation in the right side of the heart and PAs in PAH, providing insights into the remodeling of these structures. Moreover, ^{18}F-FAPI uptake may serve as a marker of disease progression. Further research is required to validate its potential for assessing disease severity and monitoring treatment efficacy.

DISCLOSURE

This work was supported by the Natural Science Foundation of Guangdong Province, China (2022A1515010472), the Science and Technology Projects in Guangzhou, China (2,02,20,10,20,558), the National Natural Science Foundation of China (8,20,01,879),

the Guangdong regional joint fund (2022A1515110941), and the Guangzhou basic and applied basic research (2023A04J1196). No other potential conflict of interest relevant to this article was reported.

KEY POINTS

QUESTION: What is the significance of ^{18}F-FAPI uptake in the right side of the heart and PA for PAH disease management?

PERTINENT FINDINGS: In an MCT-induced PAH rat model, increased FAP expression was observed in the heart and lungs, with early ^{18}F-FAPI uptake in these tissues following PAH induction, which then gradually decreased. This suggests that FAP expression is an early response to tissue remodeling in PAH. In patients with PAH, ^{18}F-FAPI uptake in the right side of the heart and PAs correlated with clinical assessments and hemodynamic parameters. Additionally, decreased ^{18}F-FAPI uptake in 3 patients with follow-up PET/CT scans was associated with clinical improvements.

IMPLICATIONS FOR PATIENT CARE: The ^{18}F-FAPI uptake in PAH showed potential for noninvasively evaluating disease severity and therapeutic response. Tracking ^{18}F-FAPI uptake could pave the way for more personalized management of PAH, offering deeper insights into disease progression and treatment effectiveness.

REFERENCES

1. Humbert M, Kovacs G, Hoeper MM, et al. ESC/ERS Scientific Document Group. 2022 ESC/ERS guidelines for the diagnosis and treatment of pulmonary hypertension. *Eur Respir J.* 2023;61:2200879.
2. Stenmark KR, Davie N, Frid M, Gerasimovskaya E, Das M. Role of the adventitia in pulmonary vascular remodeling. *Physiology (Bethesda).* 2006;21:134–145.
3. Vonk Noordegraaf A, Westerhof BE, Westerhof N. The relationship between the right ventricle and its load in pulmonary hypertension. *J Am Coll Cardiol.* 2017; 69:236–243.
4. Stewart JA, Jr, Massey EP, Fix C, et al. Temporal alterations in cardiac fibroblast function following induction of pressure overload. *Cell Tissue Res.* 2010;340:117–126.
5. Maron BA, Leopold JA. Emerging concepts in the molecular basis of pulmonary arterial hypertension: part II—neurohormonal signaling contributes to the pulmonary vascular and right ventricular pathophenotype of pulmonary arterial hypertension. *Circulation.* 2015;131:2079–2091.
6. Lindner T, Loktev A, Giesel F, et al. Targeting of activated fibroblasts for imaging and therapy. *EJNMMI Radiopharm Chem.* 2019;4:16.
7. Gu Y, Han K, Zhang Z, et al. ^{68}Ga-FAPI PET/CT for molecular assessment of fibroblast activation in right heart in pulmonary arterial hypertension: a single-center, pilot study. *J Nucl Cardiol.* 2023;30:495–503.
8. Chen BX, Xing HQ, Gong JN, et al. Imaging of cardiac fibroblast activation in patients with chronic thromboembolic pulmonary hypertension. *Eur J Nucl Med Mol Imaging.* 2022;49:1211–1222.
9. Xing HQ, Gong JN, Chen BX, et al. Comparison of ^{68}Ga-FAPI imaging and cardiac magnetic resonance in detection of myocardial fibrosis in a patient with chronic thromboembolic pulmonary hypertension. *J Nucl Cardiol.* 2022;29: 2728–2730.
10. Nogueira-Ferreira R, Vitorino R, Ferreira R, et al. Exploring the monocrotaline animal model for the study of pulmonary arterial hypertension: a network approach. *Pulm Pharmacol Ther.* 2015;35:8–16.
11. Zeng X, Zhao R, Wu Z, et al. [^{18}F]-FAPI-42 PET/CT assessment of progressive right ventricle fibrosis under pressure overload. *Respir Res.* 2023;24:270.
12. Li Y, Lin X, Li Y, et al. Clinical utility of F-18 labeled fibroblast activation protein inhibitor (FAPI) for primary staging in lung adenocarcinoma: a prospective study. *Mol Imaging Biol.* 2022;24:309–320.
13. Lin JL, Chen HM, Lin FC, et al. Application of DynaCT angiographic reconstruction in balloon pulmonary angioplasty. *Eur Radiol.* 2020;30:6950–6957.
14. Zhou YP, Wei YP, Yang YJ, et al. Percutaneous pulmonary angioplasty for patients with Takayasu arteritis and pulmonary hypertension. *J Am Coll Cardiol.* 2022;79:1477–1488.
15. Song W, Zhang X, He S, et al. ^{68}Ga-FAPI PET visualize heart failure: from mechanism to clinic. *Eur J Nucl Med Mol Imaging.* 2023;50:475–485.
16. Stenmark KR, Fagan KA, Frid MG. Hypoxia-induced pulmonary vascular remodeling: cellular and molecular mechanisms. *Circ Res.* 2006;99:675–691.
17. Stenmark KR, Yeager ME, El Kasmi KC, et al. The adventitia: essential regulator of vascular wall structure and function. *Annu Rev Physiol.* 2013;75:23–47.
18. Andersen S, Nielsen-Kudsk JE, Vonk Noordegraaf A, et al. Right ventricular fibrosis. *Circulation.* 2019;139:269–285.
19. Thenappan T, Chan SY, Weir EK. Role of extracellular matrix in the pathogenesis of pulmonary arterial hypertension. *Am J Physiol Heart Circ Physiol.* 2018;315: H1322–H1331.
20. Borgdorff MA, Bartelds B, Dickinson MG, et al. Sildenafil treatment in established right ventricular dysfunction improves diastolic function and attenuates interstitial fibrosis independent from afterload. *Am J Physiol Heart Circ Physiol.* 2014;307: H361–H369.
21. Gomez-Arroyo J, Sakagami M, Syed AA, et al. Iloprost reverses established fibrosis in experimental right ventricular failure. *Eur Respir J.* 2015;45:449–462.
22. Savale L, Guignabert C, Weatherald J, Humbert M. Precision medicine and personalising therapy in pulmonary hypertension: seeing the light from the dawn of a new era. *Eur Respir Rev.* 2018;27:180004.